J Therm Anal Calorim (2018) 131:811–822
https://doi.org/10.1007/s10973-017-6270-z

Thermal decomposition kinetics of sugarcane mills wastes

Daniel R. da Silva[1] · Marisa S. Crespi[1] · Clóvis A. Ribeiro[1] · Jorge M. V. Capela[1]

Received: 11 August 2016 / Accepted: 6 March 2017 / Published online: 14 March 2017

Abstract The aim of this work was to evaluate the kinetic parameters regarding the first thermal decomposition mass loss step of organic matter present in samples of bagasse, filter cake, and vinasse provided by two sugarcane mills by TG in pyrolysis and combustion conditions. LL-INT Wanjun–Donghua procedure modified by Capela–Ribeiro was employed to estimate activation energy in function of the extent of conversion. The chemical composition of samples was determined by ultimate analysis, FTIR spectroscopy, X-ray diffractometry, and atomic absorption spectrophotometry among other analytical techniques. Results indicated that despite similar organic composition, the energetic potential of filter cake and vinasse was lower than that of bagasse due to their increased inorganic content. Filter cake presented high amounts of Ca, Cu, Fe, Mn, P, and Zn. Vinasse showed greater concentrations of Na and K and higher amounts of other metals such as Ca, Mg, Mn and Zn than bagasse and filter cake samples. Filter cake and vinasse samples had significant concentrations of heavy metals like Cr and Pb. However, considerable differences were observed when the chemical composition of samples from a same type of waste was compared. Different kinetic mechanisms of reaction were observed for a same kind of waste which resulted in variation of mean activation energy values. Regarding this parameter, samples that were subjected to nucleation presented lower values than the ones that showed geometrical contraction. The order-based models were responsible for the elevation of activation energy. Despite these facts, the kinetic compensation effect was observed for all samples in both pyrolysis and combustion atmospheres.

Keywords Sugarcane · Bagasse · Vinasse · Filter cake · Thermal decomposition kinetics

Introduction

The energetic demand is increasing due to population growth and industrialization. Conventional energy sources have limited reserves and should not last much longer [1]. It is estimated that current reserves of coal, oil, and natural gas will last for another 218, 41 and 63 years, respectively, if the present demand remains constant. Renewable energy sources should be playing a crucial role regarding power generation in the next years [2–4].

Plentiful biomass in Brazil is sugarcane and the wastes generated by sugarcane mills. Bagasse and filter cake, also known as press mud, are solid by-products of sugar and ethanol production [5]. Vinasse is a liquid waste from alcoholic fermentation of sugarcane juice for ethanol production [6]. A ton of milled cane generates about 250–290 kg of bagasse and 30–40 kg of filter cake [5, 7, 8]. A liter of produced ethanol yields around 7–14 L of vinasse [9].

The use of bagasse as a fuel depends on its heating capacity, which is a consequence of its physical–chemical composition. Energy generation from bagasse is well established for decades in Brazil. Vinasse and filter cake have usually been applied as fertilizers on sugarcane crops due to their high concentration of phosphorous and

Electronic supplementary material The online version of this article (doi:10.1007/s10973-017-6270-z) contains supplementary material, which is available to authorized users.

✉ Marisa S. Crespi
crespims@iq.unesp.br

[1] Institute of Chemistry, São Paulo State University (UNESP), R. Prof. Francisco Degni 55, Araraquara, SP, Brazil

potassium [10]. However, such activity might cause several changes in soil such as elevation of pH, salinization, and leaching of metals to underground waters [11, 12]. An alternative use of these wastes is anaerobic digestion for biogas generation [13]. Despite promising results, this process still presents some drawbacks like the production of corrosive gases such as H_2S [14].

Pyrolysis of biomass is considered as the thermal decomposition of organic matter in the absence of oxygen-generating liquid and gaseous products in addition to a carbonaceous solid, known as biochar. Large hydrocarbon molecules are degraded to smaller ones. Such process usually starts at 300 °C and is still observed until 600 or 700 °C [2, 15]. Combustion is the thermal decomposition of organic matter in the presence of oxygen-generating CO_2, water, and heat as products. Biomass constituents play a crucial role in its combustion process since the amount of released heat is heavily influenced by them. Due to its high volatility and reactivity, biomass is one of the best raw materials for combustion [16]. However, incomplete combustion of biomass generates substantial amounts of several pollutants such as CO and particulate matter [17]. Furthermore, low efficiency of the process, ash sinterization, and fouling in addition to large quantities of ashes produced by some biomasses are problems regarding this process [18]. Also, biomass presents lower amounts of carbon, aluminum and iron, inferior higher heating values, and density in addition to increased contents of oxygen, potassium, silicon, and moisture when compared to fossil fuels [13, 16, 19]. The presence of alkali metals and chlorine in biomass may derail the use of produced ashes in construction materials [20]. Chlorine present in the ashes interacts with alkali metals, enhancing their mobility by the generation of alkali chlorides with low melting points. Such compounds leave the ashes as volatile gasses that cause direct corrosion by accelerating the oxidation of metal alloys [21, 22].

There are many books and reports regarding solid-state reactions and the mechanisms controlling them [23–27]. Some of these mechanisms (*A*, *R* and *F*) and the kinetic compensation effect (KCE) are quickly described in the next section.

Avrami–Erofeev nucleation models (*A*)

Since fractures and displacements caused by impurities and defects situated in surface or edges might affect local energies in solids, nuclei growth is favored over these points, which are known as nucleation sites. According to De Bruijn et al. [27], Eq. 1 describes solid-state isothermal reactions involving nuclei formation and growth:

$$[-\ln(1-\alpha)]^{1/n} = kt \tag{1}$$

However, in non-isothermal conditions, derivative of Eq. 2 should be used:

$$\frac{d\alpha}{1-\alpha} = kn[-\ln(1-\alpha)]^{1-1/n}dt \tag{2}$$

In both equations, $n = \beta + \gamma$, where β is the number of significant successive events to generate a growth nucleus, and γ is the growth dimensions index (1, 2 or 3).

Geometrical contraction models (*R*)

Assuming that nucleation takes place quickly over the solid's surfaces, the reaction rate is controlled by the advance of reaction interface into the center of such solid particle. When reaction occurs only in certain solid faces, the area contracting equation (Eq. 3), also known as contracting cylinder equation or R2 kinetic model, describes the reaction rate [23–25]:

$$1-(1-a)^{1/2} = kt \tag{3}$$

If the reaction occurs equally in every surface of a cube of edge a, volume of non-reacted solid is a cube of edge $a - 2kgt$. Thus, the volume contracting equation (Eq. 4), also known as contracting cube or sphere (R3 kinetic model), can be derived:

$$a = \frac{a^3 - (a-2kgt)^3}{a^3} \quad \text{and} \quad 1-(1-a)^{1/3} = kt \tag{4}$$

Reaction-order models (*F*)

Presuming that the reaction rate is directly proportional to the remaining concentration of the solid reactant raised to an integral or fractional power, which is known as reaction order (n), these models are derived from Eq. 5 [23, 24]:

$$\frac{d\alpha}{dt} = k(1-\alpha)^n \tag{5}$$

Considering $n = 1$, F1 kinetic model or Mampel model is obtained (Eq. 6):

$$\frac{d\alpha}{dt} = k(1-\alpha) \rightarrow -\ln(1-\alpha) = kt \tag{6}$$

For $n = 2$, Eq. 7 results (F2 kinetic model):

$$\frac{d\alpha}{dt} = k(1-\alpha)^2 \rightarrow \left[\frac{1}{(1-\alpha)}\right] - 1 = kt \tag{7}$$

Kinetic compensation effect (KCE)

This effect was first detected by Zawadski and Bretsznajder in 1935 when studying $CaCO_3$ thermal decomposition in CO_2 atmosphere [25]. In that work, elevation of the partial

pressure of carbon dioxide resulted in an increase of activation energy. KCE establishes that, even if activation energy of a reaction is increased, the rate in which it occurs will not be affected due to a compensatory effect of A, pre-exponential factor in Arrhenius Equation (Eq. 8) [25, 28].

$$\ln A = a + bE_a \quad (8)$$

In Eq. 8, $a = k_{iso}$ and $b = \frac{1}{RT_{iso}}$. T_{iso} is considered as isokinetic temperature, which is the temperature where a set of reactions takes place in a same rate k_{iso}. This group of reactions exhibits a linear relationship between ln$A$ and E_a.

Isoconversional methods and kinetic study of sugarcane mills wastes

Several isoconversional methods were proposed to estimate activation energy (E) as a function of the extent of conversion (α). However, according to Wanjun and Donghua [29], if a variation of E values as conversion proceeds is observed, Friedman differential method [30] presents estimates of E that differ from the ones given by isoconversional integral methods such as Kissinger–Akahira–Sunose [31], Flynn–Wall–Ozawa [32, 33], Li-Tang [34] and Vyazovkin's "Model-Free" [35]. Since such isoconversional integral methods assume that E and A are constant with the extent of conversion, a systematic error is introduced if E varies with α. In Friedman method, this error is not included. Wanjun and Donghua proposed a local linear integral isoconversional (LL-INT) procedure to evaluate the activation energy dependence in non-isothermal conditions. That method does not introduce a systematic error, as previously discussed, like other integral isoconversional procedures [29].

Considering the evaluation of kinetic parameters involving thermal decomposition of sugarcane mills wastes, pyrolysis of bagasse was studied in nearly all works regarding this subject [36–39]. Concerning the first thermal degradation step of organic matter, several works used different isoconversional methods to estimate activation energy. Ounas et al. [36] detected activation energy values of 163–173 and 176–184 kJ mol^{-1} employing Flynn–Wall–Ozawa and Vyazovkin's "Model-Free" methods, respectively. Aboyade et al. [37] detected an interval of 180–200 kJ mol^{-1} for activation energy by Friedman method. Mothé and Miranda observed values between 110–200 kJ mol^{-1} (Friedman) and 110–160 kJ mol^{-1} (Flynn–Wall–Ozawa) [38]. Motaung and Anandjiwala used Flynn–Wall–Ozawa and Kissinger–Akahira–Sunose procedures to estimate activation energy ranging from 100 to 120 kJ mol^{-1} in the same conditions [39].

Gangavati et al. [40] employed other methods such as Coats and Redfern [41], Agrawal and Subramanian [42], Freeman and Carroll [43], Horowitz and Metzger [44], Reich and Stivala [45] and Piloyan and Novikova [46] to assess kinetic parameters of pyrolysis of filter cake. With a heating rate of 20 °C min^{-1}, the activation energy of this sample ranged from 7.91 to 75.12 kJ mol^{-1}. The authors also observed a 72.25 kJ mol^{-1} value in a 40 °C min^{-1} by Agrawal and Subramanian method. Regarding thermal oxidation of filter cake, a 105.79 kJ mol^{-1} value was estimated in 20 °C min^{-1}, while a 21.71 kJ mol^{-1} activation energy was observed in 40 °C min^{-1} (both using Agrawal and Subramanian method).

However, no reports were found concerning the thermal decomposition kinetics of vinasse. Considering this lack of works aiming the evaluation of thermal degradation kinetics in pyrolysis and combustion conditions of sugarcane mills wastes, this study used the LL-INT Wanjun–Donghua procedure [29] with some modifications by Capela–Ribeiro in order to assess the kinetic parameters regarding the first decomposition step of organic matter present in bagasse, filter cake, and vinasse samples on pyrolysis and combustion atmospheres by TG curves.

Experimental

Sample preparation

Bagasse, filter cake and vinasse were obtained from two sugarcane mills situated near Araraquara City (−21°47′40″S, 48°10′32″W, elevation of 664 m), state of São Paulo, Brazil. The sugarcane plants (*Saccharum officinarum*) were harvested at an age of 12 months, approximately. They were milled in sugarcane mills, removing the juice out of the shredded pulp (bagasse), which was used in this study. The juice, after several steps, generates, as by-products, filter cake (from sugar production) and vinasse (from ethanol production).

All samples were labeled as A or B (Bagasse A, Bagasse B, etc.), according to their origin. They were prepared by washing with distilled water at room temperature (except vinasse) and drying at 80 °C to remove moisture. Then, they were ground or milled by a hand mortar followed by sieving to obtain particles with dimensions around 90 μm. To determine the main constituents present in the inorganic matter of samples, the procedure regarding sample digestion that was used in this work was proposed by Jesus et al. [47] and was detailed by Silva et al. [48].

Sample characterization

Determination of inorganic matter was performed by flame photometry (Micronal® B262 Flame Photometer)—Na and K; atomic absorption spectrophotometry (Varian®

SpectrAA 240 FS)—Al, Ca, Fe, and Mg; and vis-spec, using Eaton, Clesceri, and Greenberg [49] method (Femto® 435 spectrophotometer)—P. FTIR spectra of samples were acquired by using a Perkin Elmer® Spectrum 2000 spectrophotometer. The pellets were made by mixing each biomass sample with KBr at a 10:1 (m/m) ratio. The obtained spectrum for each sample was the average of 16 scans in the IR range of 400–4000 cm^{-1} at 2 cm^{-1}. A TOPCON® SM-300 performed scanning electronic microscopy (SEM) with 100×, 500×, and 1000× magnifications with an acceleration voltage of 10 kV. The ultimate analysis was performed using a CE Instruments® EA 1110 CHNS-O analyzer. Higher heating values (HHV) were acquired by an IKA-WERKE® C2000 calorimetric bomb. Using a modification of Dulong's equation [50], HHVs were also estimated by ultimate analysis results according to the following expression (Eq. 9):

$$\mathrm{HHV}\left(\mathrm{MJ\,kg^{-1}}\right) = 33.5(\%\mathrm{C}) + 142.3(\%\mathrm{H}) - 15.4(\%\mathrm{O}) \tag{9}$$

Thermal characterization and determination of kinetic parameters

Thermogravimetric analysis (TG) was performed by a simultaneous SDT-2960 modulus (TA Instruments®). For pyrolysis and combustion studies, N_2 and synthetic air atmospheres, respectively, were employed at a flow of 100 mL min^{-1}. A mass of 6.0 ± 0.5 mg of each sample was heated from room temperature to 600 °C at several heating rates (10, 15, 20, 25, and 30 °C min^{-1}).

To assess the kinetic parameters regarding the first decomposition step of organic matter of each sample, LL-INT Wanjun–Donghua method [29] modified by Capela–Ribeiro was used. Such method assumes that, on non-isothermal conditions, the rate in which a solid-state reaction takes place can be described by (Eq. 10):

$$\frac{\mathrm{d}\alpha}{\mathrm{d}T} = \frac{A}{\beta}\exp\left(-\frac{E}{RT}\right)f(\alpha) \tag{10}$$

In that equation, α is the conversion factor, T is the temperature, R is the gas constant, A is the frequency factor, E is the activation energy, and $f(\alpha)$ is the differential reaction kinetic model. Cai and Liu [51] proposed an expression for $f(\alpha)$ (Eq. 11):

$$f(\alpha) = \alpha^{\mathrm{r}}(1-q\alpha)^{\mathrm{s}} \tag{11}$$

According to them, r, s, and q could be estimated by plotting $f(\alpha)/f(0.5)$. After that normalization, several $f(\alpha)$ functions were adjusted to Eq. 11 to assess r, s, and q parameters. Table 1S displays the general empirical kinetic model and r, s, and q for some solid-state kinetic models. Assuming that E_α, A_α, and β_α are constant in $[\alpha-\Delta\alpha, \alpha+\Delta\alpha]$ interval, integration of Eq. 10 results, after separation of variables, in (Eq. 12):

$$\Delta g(\alpha) = \int_{\alpha-\Delta\alpha}^{\alpha+\Delta\alpha}\frac{1}{f(\alpha)}\mathrm{d}\alpha = \frac{A_\alpha}{\beta_\alpha}\int_{T\alpha-\Delta\alpha}^{T\alpha+\Delta\alpha}\exp(-E_\alpha/RT)\mathrm{d}T \tag{12}$$

where $\Delta g(\alpha) = g(\alpha+\Delta\alpha) - g(\alpha-\Delta\alpha)$ and $g'(\alpha) = \frac{1}{f(\alpha)}$. The g function is known as integral kinetic model.

Using the Mean Value Theorem to the integral function on the right side of Eq. 12 and the Taylor series expansion around T_α in $\mathrm{e}^{-\mathrm{E}_\alpha/\mathrm{RT}}$, we obtain:

$$\frac{\beta_\alpha}{\Delta T_\alpha(1+\gamma)} = \frac{A_\alpha}{\Delta g(\alpha)}\mathrm{e}^{-\mathrm{E}_\alpha/\mathrm{RT}} \tag{13}$$

where

$$\Delta T_\alpha = T_{\alpha+\Delta\alpha} - T_{\alpha-\Delta\alpha} \tag{14}$$

$$\gamma = \frac{E_\alpha}{RT_\alpha^2}(\tau_\alpha - T_\alpha) + \left(\frac{E_\alpha^2 - 2E_\alpha RT_\alpha}{R^2T_\alpha^4}\right)(\tau_\alpha - T_\alpha)^2 \tag{15}$$

$$\tau_\alpha = -\frac{E_\alpha}{R[\ln I(\alpha) - \ln \Delta T_\alpha]} \tag{16}$$

with $I(\alpha)$ being the exponential integral in Eq. 12.

Applying a logarithm to Eq. 13, the following linear relation is obtained (Eq. 17):

$$\ln\left[\frac{\beta_\alpha}{\Delta T_{\alpha(1+\gamma)}}\right] = \beta_\alpha - \frac{E_\alpha}{RT_\alpha} \tag{17}$$

where $\beta_\alpha = \ln\frac{A_\alpha}{\Delta g(\alpha)}$, which results in (Eq. 18):

$$A_\alpha \approx \frac{2\Delta \propto \mathrm{e}^{B_\alpha}}{f(\alpha)} \tag{18}$$

Considering a conversion degree α and a series of $n \geq 3$ non-isothermal experiments performed at several heating rates $\beta_{\alpha,\mathrm{i}}$, $i = 1, 2, \ldots, n$, Eq. 17 could be used to develop a local integral isoconversional method comprised in $[\alpha-\Delta\alpha, \alpha+\Delta\alpha]$ conversion interval. Such method starts by evaluating the dispersion plot of $\ln[\beta_{\alpha,\mathrm{i}}(\Delta T_{\alpha,\mathrm{i}}(1+\gamma_\mathrm{i})]$ versus $1/RT_{\alpha,\mathrm{i}}$ to $\gamma_\mathrm{i} = 0$, $i = 1, 2, \ldots, n$. E_α and B_α can be estimated from the slope and intercept, in that order, of the straight line obtained. Replacing those values in Eq. 15, new values of γ_i are calculated, allowing obtaining new estimates to E_α and B_α. That process is repeated until convergence of the estimates for E_α and B_α is observed.

From Eqs. 10 and 12, the following expression results to each α in a non-isothermal experiment (Eq. 19):

$$\Delta f(\alpha)\Delta g(\alpha) = \left[\frac{\mathrm{d}\alpha}{\mathrm{d}T}\Big|_{T_{\alpha+\Delta\alpha}}\mathrm{e}^{\mathrm{E}_\alpha/\mathrm{RT}_{\alpha+\Delta\alpha}} - \frac{\mathrm{d}\alpha}{\mathrm{d}T}\Big|_{T_{\alpha-\Delta\alpha}}\mathrm{e}^{\mathrm{E}/\mathrm{RT}_{\alpha-\Delta\alpha}}\right]I(\alpha) \tag{19}$$

where $\Delta f(\alpha) = f(\alpha+\Delta\alpha) - f(\alpha-\Delta\alpha)$, $I(\alpha)$ is the exponential integral in Eq. 12, and the subscript indicates the

temperature in which derivatives are calculated. Considering the approximation $\Delta f(\alpha)\cdot\Delta g(\alpha)\approx 4(\Delta\alpha)^2 f'(\alpha)/f(\alpha)$ and the general kinetic empirical model $f(\alpha)=\alpha^r(1-q\alpha)^s$, we obtain (Eq. 20):

$$\frac{(r+s)q\alpha - r}{q\alpha^2-\alpha} = \frac{1}{4(\Delta\alpha)^2}\Delta f(\alpha)\Delta g(\alpha) \quad (20)$$

Parameters of $f(\alpha)$ function are calculated by minimization of the next sum of squares in relation to r, s, and q (Eq. 21):

$$SQ(r,s,q) = \sum_j \left[\frac{(r+s)q\alpha_j - r}{q\alpha_j^2 - a_j} - \frac{1}{4(\Delta\alpha_j)^2}\Delta f(a_j)\Delta g(a_j)\right]^2 \quad (21)$$

Results and discussion

Sample composition

It can be seen from an analysis of Fig. 1 that bagasse samples presented the highest carbon (47.74%, Bagasse A), hydrogen (7.41%, Bagasse A), and oxygen (47.43%, Bagasse B) concentrations among the studied wastes. Besides, lowest ash contents (0.57 and 3.19% for Bagasse A and Bagasse B, respectively) were detected for them in comparison with filter cake and vinasse samples. Consequently, about higher heating values, bagasse samples exhibited superior values (17.31 ± 0.21 MJ kg^{-1} for Bagasse A and 17.82 ± 0.06 MJ kg^{-1} for Bagasse B) among all studied wastes. Moreover, it was verified that Bagasse B was constituted by lower carbon (38.08%) and hydrogen (6.42%) concentrations when compared to Bagasse A. Since such sample was characterized by higher oxygen and ash contents, estimated HHV of Bagasse B (14.6 MJ kg^{-1}) was lower than estimated HHV for Bagasse A (20.6 MJ kg^{-1}). However, such fact was not observed experimentally. Considering that the modification of Dulong's equation used in this work (Eq. 9) is an approximation, it should be employed with caution.

Vinasse samples were constituted by the lowest carbon (30.79 and 29.46% for Vinasse A and Vinasse B, in that order) and hydrogen (6.23% for Vinasse A) concentrations in addition to a high ash content (34.44%), resulting in the lowest values for higher heating value (12.18 ± 0.08 MJ kg^{-1} for Vinasse A and 11.34 ± 0.02 MJ kg^{-1} for Vinasse B) when compared to bagasse and filter cake samples. Taking into account that both vinasse samples did not present significant variations between their C, H, N, S and O constitutions, similar estimated HHVs were observed for them, slightly higher for Vinasse A (16.0 MJ kg^{-1}) in relation to Vinasse B (15.9 MJ kg^{-1}).

Same factors, especially the high ash content (34.16 and 24.18% for Filter Cake A and Filter Cake B, respectively), were crucial for a lower HHV determined to both of these samples (14.60 ± 0.12 MJ kg^{-1} for Filter Cake A and 16.70 ± 0.12 MJ kg^{-1} for Filter Cake B) when compared to bagasse samples. Besides, the higher carbon concentration detected for Filter Cake B (38.26%) and lower ash content in comparison with Filter Cake A, which carbon concentration was 35.95%, resulted in a lower value of HHV for the latter, both estimated (18.5 MJ kg^{-1}—Filter Cake A; 18.7 MJ kg^{-1}—Filter Cake B) and experimentally obtained.

In relation to other inorganic elements, vinasse samples presented the highest amounts of sodium (21.9 ± 1.1 g kg^{-1}—Vinasse A and 20.9 ± 1.2 g kg^{-1}—Vinasse B) and potassium (110 ± 58 and 103 ± 40 g kg^{-1} for Vinasse A and Vinasse B, respectively), filter cake samples were constituted by a significant concentration of phosphorous (3.72 ± 0.69 g kg^{-1}, Filter Cake A), and the lowest contents of inorganic matter were detected for bagasse samples.

Bagasse samples did not present significant variations regarding macronutrient (Al, Ca, Fe K, Mg, Na, and P) contents between each other. However, such tendency was not seen for A and B samples of Filter Cake and Vinasse. Filter Cake A had a Fe concentration (12.3 ± 0.3 g kg^{-1}) much higher than the one detected for Filter Cake B (1.10 ± 0.03 g kg^{-1}). Potassium and phosphorous concentrations were also present in greater values in Filter Cake A in relation to Filter Cake B, as shown in Table A1. Filter Cake B presented a greater content of Ca in relation to Filter Cake A (27.0 ± 2.0 and 15.5 ± 1.8, both in g kg^{-1}, respectively). Considering vinasse samples, concentration of Fe in Vinasse A (1.48 ± 0.01 g kg^{-1}) was higher when compared to the amount verified for this metal in Vinasse B (0.26 ± 0.03 g kg^{-1}). Aluminum was also detected in a larger concentration in Vinasse A in comparison with Vinasse B (0.80 ± 0.02 and 0.12 ± 0.02 g kg^{-1}, in that order).

Concentration of micronutrients (Cr, Cu, Mn, Ni, Pb and Zn) presented variations between A and B samples of a same type of waste. Bagasse A had a lower content of Zn (2.57 ± 0.42 mg kg^{-1}) in relation to the B sample (3.97 ± 0.42 mg kg^{-1}). Bagasse B also had a sixteen times higher Cr concentration (32.8 ± 5.44 mg kg^{-1}) and forty times greater Ni content (13.4 ± 11.0 mg kg^{-1}) was detected when compared to Bagasse A (Cr: 2.12 ± 1.13 mg kg^{-1}; Ni: 0.33 ± 0.00 mg kg^{-1}). Conversely, Pb concentration detected for Bagasse B (6.50 ± 0.71 mg kg^{-1}) was lower than the one found in Bagasse A (13.5 ± 2.83 mg kg^{-1}). Filter Cake A had greater contents of Cu (61.0 ± 3.0 mg kg^{-1}), Mn (1.03 ± 0.05 g kg^{-1}), Ni (19.5 ± 4.4 mg kg^{-1}), and Pb (43.0 ± 9.2 mg kg^{-1}) than Filter Cake B (Cu:

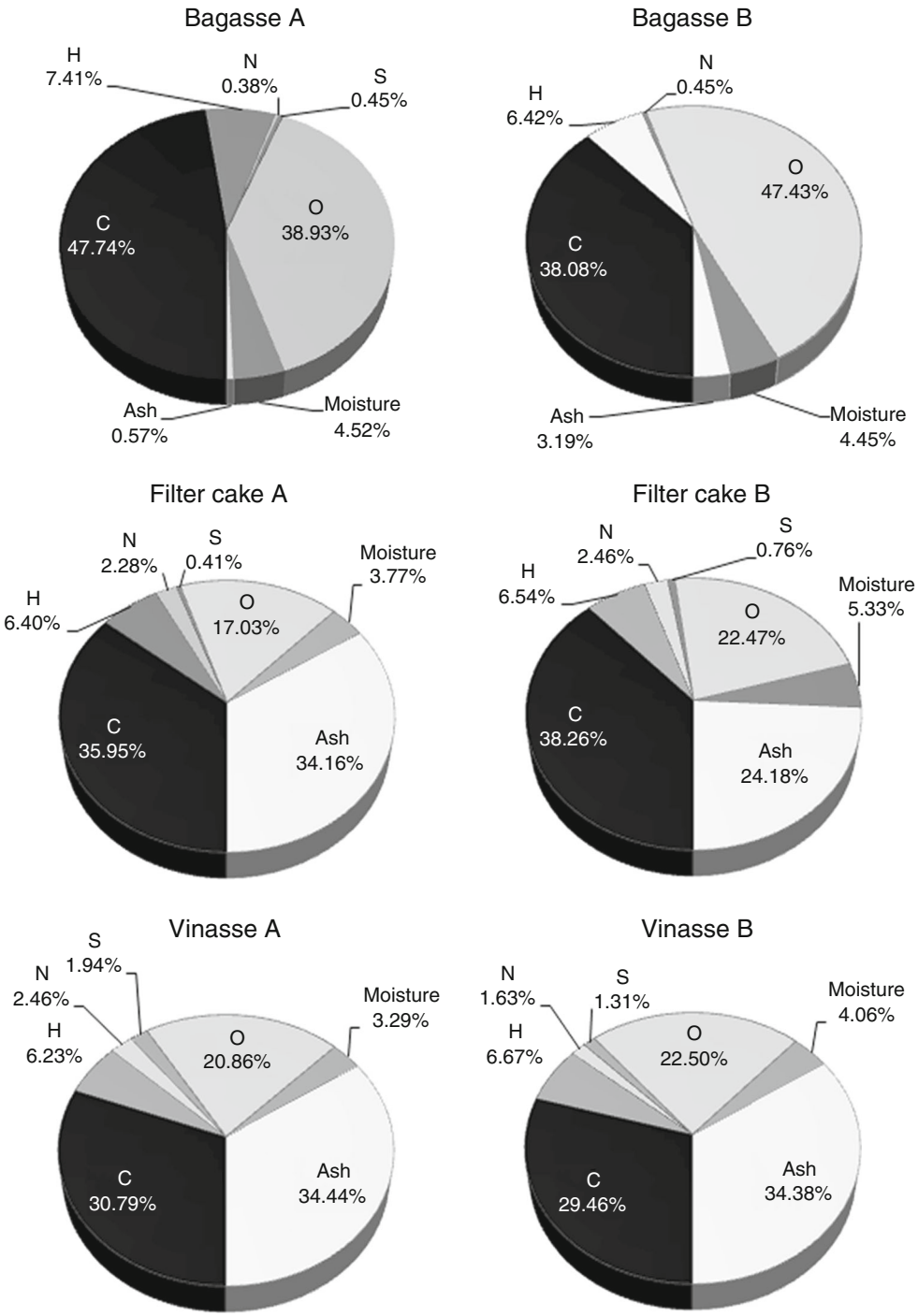

Fig. 1 Ultimate analysis of studied samples

40.0 ± 0.9 mg kg^{-1}; Mn: 847 ± 26 mg kg^{-1}, Ni: 10.6 ± 0.2 mg kg^{-1}; Pb: 25.5 ± 2.1 mg kg^{-1}). Micronutrients were present in higher amounts in Vinasse A, in comparison with Vinasse B, especially Cr (Vinasse A: 49.0 ± 0.8 mg kg^{-1}; Vinasse B: 10.2 ± 4.4 mg kg^{-1}) and Pb (Vinasse A: 30.5 ± 8.7 mg kg^{-1}; Vinasse B: 6.0 ± 9.6 mg kg^{-1}), both five times greater, and Mn (Vinasse A: 361 ± 20 mg kg^{-1}; Vinasse B: 138 ± 6 mg kg^{-1}), two and a half times higher.

The high contents of calcium found in both filter cake and vinasse samples resulted from clarification of sugarcane juice during the production of sugar and ethanol in the sugarcane mills [52]. Such process consisted in adding CaO or $Ca(OH)_2$ to coagulate and promote decantation of impurities soluble in the juice. Further information about constitution of samples, as well as FTIR, SEM and XRD results, can be consulted in Appendix 1 of Supplementary Material. Also, Appendix 2 of Supplementary Material

presents PCA plots which exhibit how sample constitution, especially C, H, N, S, O, phosphorous, and metals, affected HHVs of the studied samples. It can be seen that the presence of great amount of inorganic matter reduced the HHV of filter cake and vinasse sample in relation to bagasse samples due to ash generation after heating, affecting the energy generation potential of such wastes.

Thermal decomposition of samples

Silva et al. [48] described the thermal decomposition behavior regarding A samples (Bagasse A, Filter Cake A, and Vinasse A), both in pyrolysis and combustion conditions. Every sample exhibited a moisture loss at the beginning of their degradation in both studied atmospheres. In N_2 atmosphere, organic matter was usually decomposed in two mass loss steps (Fig. 2a), while in a synthetic air atmosphere, three mass loss steps were detected (Fig. 2b). Both vinasse samples began earlier to be degraded in comparison with bagasse and filter cake samples, regardless of the reaction atmosphere employed. Probably because a non-fibrous material such as vinasse allows fast volatilization of products since organic matter is not contained in a rigid structure, lower temperatures were necessary to start their decomposition. Because of the higher inorganic content of filter cake and vinasse samples, the final residual mass was greater for these wastes of bagasse samples.

Assessment of kinetic parameters

LL-INT Wanjun–Donghua procedure [29] modified by Capela–Ribeiro was used to determine kinetic parameters regarding the first decomposition step of organic matter for every sample on pyrolysis and combustion atmospheres. Also, a kinetic model was proposed to describe how a sample was decomposed in these conditions. Figure 3 displays how increment of heating rate affected the TG curves. Bagasse B in N_2 atmosphere is shown, as an example.

Pyrolysis of bagasse

The beginning of pyrolysis presented differences when bagasse samples were heated. Bagasse A displayed an increment of activation energy as conversion advanced (Fig. S3A). However, for Bagasse B, this parameter presented stability with few variations. Plots of lnA in function of E are presented in Supplementary Material. It can be seen that, regarding pyrolysis of Bagasse A (Fig. S1A), an elevation of lnA values was detected. Still, dispersion of

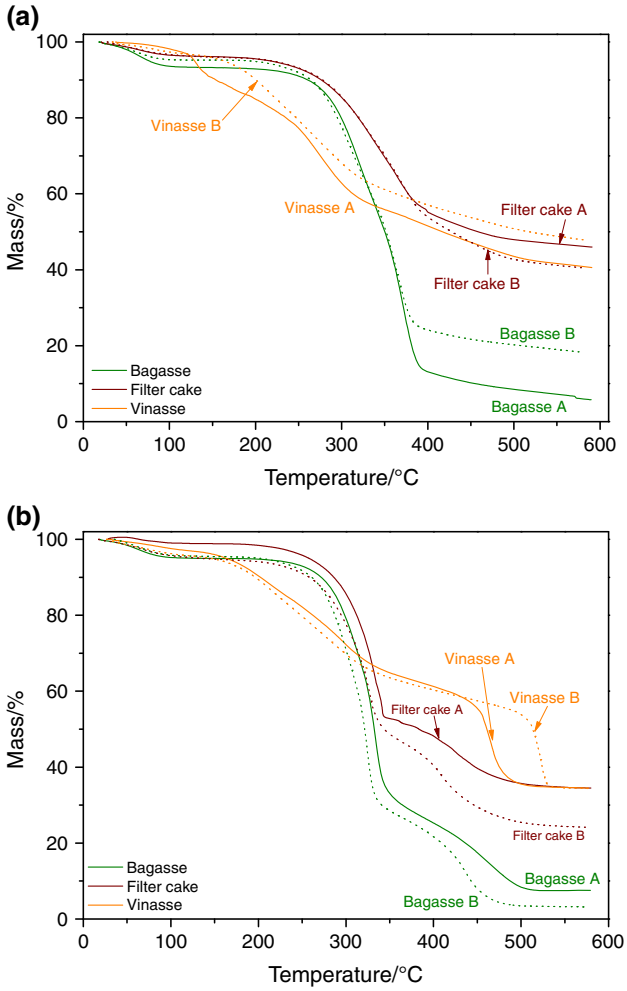

Fig. 2 TG curves of samples A (*line*) and samples B (*dotted line*) in atmosphere of **a** N_2 and **b** synthetic air

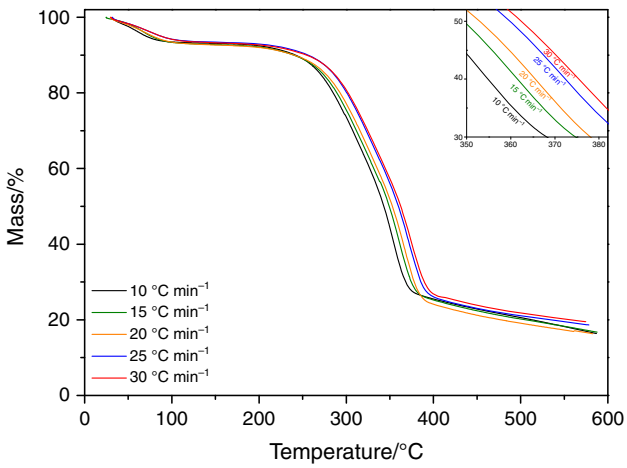

Fig. 3 TG curves of Bagasse B in N_2 atmosphere in several heating rates

lnA values around a constant could be seen for Bagasse B (Fig. S1B).

Fig. S3B and S3C show that $f(\alpha)/f(0.5)$ was reduced with the progression of conversion factor α. Such feature was detected for both bagasse samples. The curves presented a high resemblance with normalized curves of geometric conversion kinetic models. Decomposition of Bagasse A can be related to the R2 kinetic model. Bagasse B normalized curve was very similar to R3 kinetic model until $\alpha = 0.5$. From this point, R2 model was the most appropriate to describe the degradation of that sample.

Pyrolysis of filter cake

As it was previously observed to bagasse samples, a difference was detected when filter cake samples started to decompose in N_2 atmosphere. Meanwhile, Filter Cake A displayed an elevation of activation energy as its conversion advanced, Filter Cake B showed the stability of that parameter with α (Fig. S3D). Thus, ln$A$ versus E plots also displayed differences between them. Regarding Filter Cake A, ln$A$ increased with elevation of activation energy until a value around 165 kJ mol^{-1} was reached (Fig. S1C). Then, such trend was inverted. On the other hand, for Filter Cake B, ln$A$ values were diminished with progression of conversion factor after $\alpha = 0.4$ ($\ln A = 34.6$, $E = 158$ kJ mol^{-1}) (Fig. S1D).

Both samples showed similar $f(\alpha)/f(0.5)$ values which were reduced with α (Fig. S3E and Fig. S3F). It can be seen that, despite the fact that differences between activation energy values estimated for Filter Cake A and Filter Cake B were detected, both normalized curves presented great resemblance to F1 reaction-order model until $\alpha = 0.5$. From this point, the R3 model was most likely the mechanism in which both samples were decomposed.

Pyrolysis of vinasse

The activation energy of Vinasse A increased with the advance of conversion factor until $\alpha = 0.75$ where such trend was inverted (Fig. S3G). For Vinasse B, E versus α plot presented a crescent trend until $\alpha = 0.35$ when it tended to diminish. A common feature detected in both vinasse samples is that the E versus α plot displayed a concave aspect, denoting a reversible endothermic reaction. A similar pattern was detected for ln$A$ versus E plot of both samples (Fig. S1E and S1F).

However, $f(\alpha)/f(0.5)$ versus α showed distinct profiles to each of vinasse samples. Vinasse A displayed linearity (Fig. S3H), and, for Vinasse B, a curve with slightly sigmoid aspect was observed (Fig. S3I). The F1 reaction-order model presented high similarity with Vinasse A curve until $\alpha \leq 0.5$. After completion of 50% of this decomposition step, R3 geometric contraction model was most appropriate. For Vinasse B, the obtained normalized curve presented higher similarity with the R3 model until $\alpha = 0.75$. Then, the R2 kinetic model was a better match.

Kinetic compensation effect in pyrolysis conditions

Analysis of Table 1 shows that activation energy for the first organic matter decomposition step in N_2 atmosphere ranged from 100 to 160 kJ mol^{-1}. Besides, for a same type of waste, mean activation energy presented notable variations. Such fact can be explained by the distinct kinetic models in which the studied samples were decomposed.

Mean activation energy estimated for Bagasse A was almost 22 kJ mol^{-1} lower than the value calculated for Bagasse B. About vinasse; such difference was even more pronounced: around 51 kJ mol^{-1}. For both of those wastes, it was observed that a geometric contraction (R models) occurred during their decomposition. However, half of degradation of Vinasse A also followed the F1 kinetic model which resulted in higher activation energy considering all samples in pyrolysis conditions. About bagasse samples, Bagasse A was decomposed according to R2 model. Bagasse B also presented resemblance to R3 model.

For filter cake samples, a lower difference between mean activation energy values was verified. Filter Cake A showed a 10 kJ mol^{-1} lower value than Filter Cake B. Also, both filter cake samples in addition to Vinasse A were decomposed, in a first moment, according to F1 reaction-order model and, after half of the conversion was completed, to R3 geometric contraction model.

Despite following the same kinetic models (R2 and R3), Bagasse B and Vinasse B showed a difference of almost 34 kJ mol^{-1} between mean activation energy values detected for each of them. Such feature can be explained by the fact that vinasse samples were responsible for the lowest thermal stability among all studied samples (Fig. 2). Since the same kind of reactions took place during decomposition of both Bagasse B and Vinasse B samples, it can be assumed that the most easily degradable organic matter present in vinasse, a non-fibrous waste, resulted in lower activation energy. Still, such trend was not detected for Vinasse A, which displayed one of the highest mean activation energy values. As it was previously noticed, for this sample, a distinct kinetic model was most appropriate to describe its decomposition (F1 model), different reaction types took place, and higher mean activation energy value was detected when compared to Vinasse B.

Figure 4 displays a plot of mean values of lnA in function of mean activation energy for every sample. Despite differences in their chemical constitution, a straight line could be drawn with a high correlation factor ($r^2 = 0.942$). Since every sample had a similar organic

Table 1 Kinetic parameters of first decomposition step of organic matter on N_2 atmosphere

Sample	ΔT/°C	E/kJ mol^{-1}	ln$A$/min^{-1}	Kinetic model
Bagasse A	180–322	113.9 ± 5.6	24.36	R2
Bagasse B	195–316	135.5 ± 48.9	29.43	R2–R3
Filter Cake A	182–332	149.2 ± 36.2	32.12	F1–R3
Filter Cake B	189–329	159.6 ± 87.1	34.58	F1–R3
Vinasse A	183–305	152.8 ± 24.9	34.54	F1–R3
Vinasse B	153–277	101.3 ± 20.7	24.37	R2–R3

composition, it is likely that same kind of products were generated in that thermal decomposition step. Finally, it can be seen that samples which were decomposed according to geometric contraction models only (Bagasse A, Bagasse B, and Vinasse B) showed a lower value of mean activation energy when compared to those samples that also were degraded in accordance with F1 reaction-order kinetic model (Filter Cake A, Filter Cake B, and Vinasse A).

Combustion of bagasse

Both bagasse samples exhibited E versus α plots with a sinusoidal aspect (Fig. S4A), especially for Bagasse B. Regarding Bagasse A, such plot presented a crescent tendency until $\alpha = 0.35$ when it started to decrease until 85% of conversion was completed. Then, E again returned to ascend with the progression of the conversion factor. A similar pattern was observed for Bagasse B though the inversion points of tendency were at $\alpha = 0.15$ and $\alpha = 0.70$. Plots of ln$A$ versus E obtained for both bagasse samples demonstrated that ln$A$ was directly proportional to E (Fig. S2A and S2B). However, ln$A$ and E values estimated for Bagasse A were lower when compared to Bagasse B.

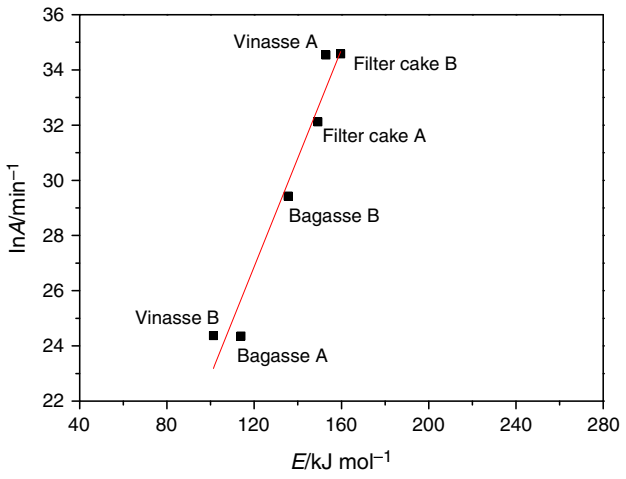

Fig. 4 Compensation plot of kinetic parameters for all samples in N_2 atmosphere

Different profiles could be seen to $f(\alpha)/f(0.5)$ versus α plots obtained for bagasse samples (Fig S4B and S4C). Meanwhile, a concave aspect was observed for Bagasse A and a decreasing curve was verified to Bagasse B. Avrami–Erofeev nucleation models (A) were the best match to explain Bagasse A decomposition reactions. The first half of degradation of this sample presented a high similarity to A1.5 kinetic model. To $\alpha > 0.5$, A4 model was a better match. Bagasse B was firstly decomposed according to F1 reaction-order model. After 50% of conversion of this sample, R3 geometric contraction model was most appropriate.

Combustion of filter cake

Filter cake samples presented distinct behaviors considering their kinetics of combustion. Analysis of Fig. S4D displayed that, for Filter Cake A, activation energy increased as conversion progressed. Such elevation was more pronounced at the end of this thermal decomposition step ($\alpha \geq 0.75$), reaching a maximum around 325 kJ mol^{-1}. For Filter Cake B, that trend was also observed until 85% of conversion was completed. From that point, activation energy values started to decrease. Besides, estimates for that parameter were lower to Filter Cake B in comparison with Filter Cake A during the whole thermal decomposition step. Such distinct behavior between those samples resulted in different profiles of ln$A$ versus E plots (Fig. S2C and S2D). Values of ln$A$ estimated to Filter Cake A increased until $\alpha = 0.20$ ($E \approx 270$ kJ mol^{-1}). An even more pronounced elevation was detected from this point to the end of conversion. About Filter Cake B, ln$A$ was directly proportional to α until this parameter was of 0.85 ($E \approx 180$ kJ mol^{-1}). Then, this tendency was inverted, and ln$A$ reached a minimum of 22.5 min^{-1} at the end of that decomposition step.

Plots of $f(\alpha)/f(0.5)$ versus α obtained for these samples presented different profiles (Fig. S4E and S4F). Despite the

fact that both curves showed a decreasing trend in a major portion of this thermal decomposition step, Filter Cake A displayed a fast descent at the beginning of conversion followed by a tendency to stability when the conversion was almost completed. An inverse trend was observed for Filter Cake B with a slight variation of $f(\alpha)$ when this sample started to decompose and a steep descent after $\alpha > 0.15$. Filter Cake A decomposition kinetics in synthetic air atmosphere took place according to F2 reaction-order model until 50% of conversion was completed. After that, F1 model presented a higher similarity. On the other hand, Filter Cake B degraded by R2 geometric contraction model.

Combustion of vinasse

Activation energy decreased as Vinasse A was decomposed until $\alpha = 0.55$ (Fig. S4G). From that point, that parameter began to rise, reaching a peak of around 130 kJ mol^{-1} at the end of the conversion. Vinasse B displayed an E versus α plot with a sigmoid aspect. Activation energy estimated for this sample showed an increase as conversion progressed, reaching around 150 kJ mol^{-1} at the end of this thermal decomposition step. For Vinasse A, there was a decrease in ln$A$ values until activation energy around 105 kJ mol^{-1} (55% of conversion factor) (Fig. S2E). Then, ln$A$ values were elevated, with a slight decrease for $0.65 \leq \alpha \leq 0.70$ ($E \approx 107$ kJ mol^{-1}). An increase of lnA was also detected to Vinasse B until $\alpha = 0.80$ ($E \approx 140$ kJ mol^{-1}) (Fig. S2F). A small decrease was seen after that point and a value of 32 min^{-1} was estimated when the conversion was completed.

Despite that distinct profiles when E versus α and ln$A$ versus E plots obtained for vinasse samples were compared, a very similar trend was seen for both when $f(\alpha)/f(0.5)$ versus α curves were plotted (Fig. S4H and S4I). However, despite both samples being decomposed according to geometric contraction models, the R2 model was most suitable to Vinasse A, and the R3 model was a better match for Vinasse B.

Kinetic compensation effect in combustion conditions

From Table 2, it can be verified that activation energy of first organic matter decomposition step ranged from 85 to 278 kJ mol^{-1}. As previously observed in pyrolysis conditions, notable differences were seen between samples A and B of bagasse and filter cake.

Mean activation energy estimated for Bagasse A was, approximately, of 125 kJ mol^{-1} lower than observed for Bagasse B. Distinct kinetic models were followed by thermal degradation of these samples. Meanwhile, Bagasse A was decomposed by Avrami–Erofeev nucleation models (A1.5 and A4) and two other models were more suitable to explain the degradation of Bagasse B: in the first moment, F1 reaction-order model and, then, R3 geometric contraction model.

Filter cake samples presented an even more pronounced difference between mean activation energy values than bagasse samples. Mean activation energy estimated for Filter Cake A was 155 kJ mol^{-1} lower in comparison with Filter Cake B. Such samples also displayed distinct behavior regarding their thermal decomposition when the reaction kinetic models most suitable for each of them were compared. For Filter Cake B, the R2 geometric contraction model was a better match. However, F1 and F2 reaction-order models were most appropriate to explain the degradation of Filter Cake A.

In contrast with observations on N_2 atmosphere, vinasse samples exhibited a slight difference between their mean activation energy values. For Vinasse A, such parameter was of 112.6 kJ mol^{-1}, around 11 kJ mol^{-1} lower than the one estimated for Vinasse B. Since these samples displayed a thermal decomposition by geometric contraction models, it was expected that this difference should be minimal. An R3 model was most appropriate for Vinasse A though the R2 model was a better match for Vinasse B.

As it was observed in pyrolysis conditions, mean ln$A$ versus mean activation energy plot was a straight line with a high correlation factor ($r^2 = 0.980$) (Fig. 5). Since

Table 2 Kinetic parameters of first decomposition step of organic matter on synthetic air atmosphere

Sample	ΔT/°C	E/kJ mol^{-1}	ln$A$/min^{-1}	Kinetic model
Bagasse A	195–297	85.6 ± 28.4	18.53	A1.5–A4
Bagasse B	193–298	201.2 ± 20.7	45.26	F1–R3
Filter Cake A	189–315	277.7 ± 68.2	61.76	F1–F2
Filter Cake B	203–321	122.4 ± 32.4	26.04	R2
Vinasse A	135–222	112.6 ± 18.2	29.40	R2
Vinasse B	150–266	123.4 ± 9.6	29.70	R3

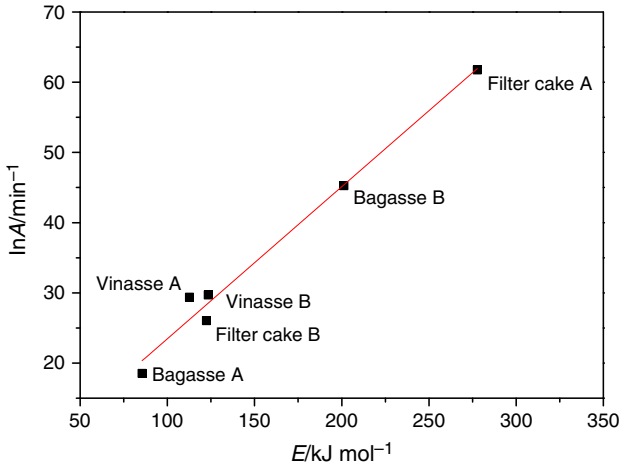

Fig. 5 Compensation plot of kinetic parameters for all samples in synthetic air atmosphere

those samples had a similar organic composition, similar products should have been generated in this thermal decomposition step for all samples. The trend that is verified in Fig. 5 was also detected in combustion conditions. Samples which were degraded according to geometric contraction models were located in a lower activation energy region than samples that were decomposed with a great resemblance to reaction-order kinetic models (Bagasse B and Filter Cake A). Besides, only comparing these two samples, Filter Cake A did not present any match with geometric contraction models and, thus, the highest mean activation energy was estimated for this sample. In the other end of the ln$A$ versus E plot, Bagasse A, which was degraded only according to Avrami–Erofeev nucleation models, displayed the lowest value for mean activation energy of all studied samples.

Conclusions

Despite similar organic composition, filter cake and vinasse samples exhibited a lower HHV than bagasse due to the presence of high amount of inorganic matter. Increased ash content detected for filter cake and vinasse affected their energy generation potential negatively.

About the first decomposition step of organic matter, Bagasse A, which was degraded by nucleation mechanisms, presented the lowest activation energy (combustion, 85.6 ± 28.4 kJ mol^{-1}) among all samples in both atmospheres. Moderate activation energy values were detected in samples that followed geometric contraction models. Samples that were decomposed according to reaction-order kinetic models displayed the higher activation energy estimates. Regardless of the reaction atmosphere, the kinetic compensation effect was observed for every studied sample.

A same type of waste presented variation in values for activation energy during thermal decomposition because different mechanisms of reaction were found for samples A and B, especially in combustion atmosphere. Hence, even if the chemical composition and thermal behavior of a sugarcane mill waste are known, a new study should be made since previous results may not apply to a sample generated by another sugarcane mill. Once wastes like filter cake and vinasse are being used as fertilizers in sugarcane crops, it is vital to know their chemical composition and rate in which such waste is decomposed, releasing heavy metals and other pollutants into soil and ground water.

Acknowledgements The authors are grateful to the Institute of Chemistry (IQ/CAr) of UNESP. We would like to thank the sugarcane mills for providing the samples used in this work. The main author would like to acknowledge Jackeline Letícia Mendonça for her great help with this work and CAPES for financial support.

References

1. Adhikari DK, Seal D, Saxena C, Goyal HB. Biomass based fuel/energy. J Petrotech Soc. 2006;3(1):28–42.
2. Goyal HB, Saxena C, Seal D. Thermochemical conversion of biomass to liquids and gaseous fuels. In: Pandey A, editor. Handbook of plant-based biofuels. Boca Raton: CRC Books; 2009. p. 30–1.
3. Chen G, Andries J, Spliethoff H. Catalytic pyrolysis of biomass for hydrogen rich fuel gas production. Energy Convers Manage. 2003;44:2289–96.
4. Hansen J, Ruedy R, Glascoe J, Sato M. GISS analysis of surface temperature change. J Geophys Res. 1999;104:30997–1002.
5. Barnes AC. The sugar cane. London: Leonard Hill; 1964. p. 365–6.
6. Mutton MA, Rossetto R, Mutton MJR. Utilização agrícola da vinhaça. In: Cortez LAB, editor. Bioetanol de cana-de-açúcar: P&D para produtividade e sustentabilidade. São Paulo: Blücher; 2010. p. 423–40.
7. Companhia Nacional de Abastecimento. A geração termoelétrica com a queima do bagaço de cana-de-açúcar no Brasil: análise do desempenho da safra 2009–2010. Brasília: CONAB; 2011. p. 157.
8. Cortez L, Magalhães P, Happi J. Principais subprodutos da agroindústria canavieira e sua valorização. Rev Bras Energia. 1992;2(2):111–46.
9. Cortez LAB, Rossell CEV, Jordan RA, Leal MRLV, Lora EES. Necessidades de P&D na área industrial de vinhaça. In: Cortez LAB, editor. Bioetanol de cana-de-açúcar: P&D para produtividade e sustentabilidade. São Paulo: Blücher; 2010. p. 183–200.
10. Ramalho JF, Amaral Sobrinho NM. Metais pesados em solos cultivados com cana-de-açúcar pelo uso de resíduos agroindustriais. Revista Floresta e Ambiente. 2001;8(1):120–9.
11. Agarwal CS, Pandey GS. Soil pollution by spent wash discharge: depletion of manganese (II) and impairment of its oxidation. J Environ Biol. 1994;15:49–53.
12. Silva MAS, Griebeler NP, Borges LC. Uso da vinhaça e impactos nas propriedades do solo e lençol freático. Revista Brasileira de Engenharia Agrícola e Ambiental. 2007;11(1):108–14.
13. Demirbas A. Fuels from biomass. In: Demirbas A, editor. Biorefineries: for biomass upgrading facilities. London: Springer; 2010. p. 33–73.

14. Cortez LAB, Silva A, Lucas J Jr, Jordan RA, Castro LR. Biodigestão de efluentes. In: Cortez LAB, Lora ES, editors. Biomassa para energia. Campinas: Editora da UNICAMP; 2007. p. 493–529.
15. Basu P. Biomass gasification and pyrolysis: practical design and theory. Burlington: Academic Press; 2010. p. 365.
16. Demirbas A. Potential applications of renewable energy sources biomass combustion problems in boiler power systems and combustion related environmental issues. Prog Energy Combust. 2005;31:171–92.
17. González JF, García CMG, Ramiro A, González J, Sabio E, Gañán J, Rodríguez MA. Combustion optimisation of biomass residue pellets for domestic heating with a mural boiler. Biomass Bioenergy. 2004;27(2):145–54.
18. Öhman M, Boman C, Hedman H, Nordin A, Bostrom D. Slagging tendencies of wood pellet ash during combustion in residential pellet burners. Biomass Bioenergy. 2004;27(6):585–96.
19. Jenkins BM, Baxter LL, Koppejan J. Biomass combustion. In: Brown RC, editor. Thermochemical processing of biomass: conversion into fuels, chemicals and power, Chapter 2. Chippenham: Antony Rowe; 2011.
20. Nussbaumer T. Combustion and co-combustion of biomass: fundamentals, technologies and primary measures for emission reduction. Energy Fuels. 2003;17:1510–21.
21. Nielsen HP, Frandsen FJ, Dam-Johansen K, Baxter LL. The implications of chlorine-associated corrosion on the operation of biomass-fired boilers. Prog Energy Combust Sci. 2000;26:283–98.
22. Backman R, Khalil RA, Todorovic D, Skreiberg O, Becidan M, Goile F, Skreiberg A, Sorum L. The effect of peat ash addition to demolition wood on the formation of alkali, lead and zinc compounds at staged combustion conditions. Fuel Process Technol. 2013;105:20–7.
23. Galwey AK, Brown ME. Theory of solid state reaction kinetics. In: Bamford CH, Tipper CFH, editors. Reaction in the solid state. Amsterdam: Elsevier; 1980. p. 41–114.
24. Galwey AK, Brown ME. Thermal decomposition of ionic solids. Amsterdam: Elsevier; 1999. p. 75–116.
25. Vyazovkin S. Some basics en route to isoconversional methodology. In: Vyazovkin S, editor. Isoconversional kinetics of thermally stimulated processes. Cham: Springer; 2015. p. 1–25.
26. Khawam A, Flanagan DR. Solid-state kinetic models basics and mathematical fundamentals. J Phys Chem B. 2006;110:17315–28.
27. De Bruijn TJW, De Jong WA, Van den Berg PJ. Kinetic parameters in Avrami-Erofeev type reactions from isothermal and non-isothermal experiments. Thermochim Acta. 1981;45:315–25.
28. White JE, Catallo WJ, Legendre BL. Biomass pyrolysis kinetics: a comparative critical review with relevant agricultural residue case studies. J Anal Appl Pyrol. 2011;91:1–33.
29. Wanjun T, Donghua C. An integral method to determine variation in activation energy with extent of conversion. Thermochim Acta. 2005;433:72–6.
30. Friedman HL. Kinetics of thermal degradation of char-forming plastics from thermogravimetry. Application to a phenolic plastic. J Polym Sci Part C. 1964;6:183–95.
31. Kissinger HE. Reaction kinetics in differential thermal analysis. Anal Chem. 1957;29:1702–6.
32. Ozawa T. A new method for analyzing thermogravimetric data. B Chem Soc Jpn. 1965;38:1881–8.
33. Flynn JH, Wall LA. A quick, direct method for the determination of activation energy from thermogravimetric data. J Polym Sci B Polym Lett. 1966;4:323–8.
34. Li CR, Tang TB. A new method for analyzing non-isothermal thermoanalytical data from solid-state reactions. Thermochim Acta. 1999;325:43–6.
35. Vyazovkin S, Wight CA. Model-free and model-fitting approaches to kinetic analysis of isothermal and nonisothermal data. Thermochim Acta. 1999;340–341:53–68.
36. Ounas A, Aboulkas A, El harfi K, Bacaoui A, Yaacoubi A. Pyrolysis of olive residue and sugar cane bagasse: non-isothermal thermogravimetric kinetic analysis. Bioresource Technol. 2011;102:11234–8.
37. Aboyade AO, Hugo TJ, Carrier M, Meyer EL, Stahl R, Knoetze JH, Görgens JF. Non-isothermal kinetic analysis of the devolatilization of corn cobs and sugar cane bagasse in an inert atmosphere. Thermochim Acta. 2011;517:81–9.
38. Mothé CG, Miranda IC. Study of kinetic parameters of thermal decomposition of bagasse and sugarcane straw using Friedman and Ozawa–Flynn–Wall isoconversional methods. J Therm Anal Calorim. 2013;113:497–505.
39. Motaung TE, Anadjiwala RD. Effect of alkali and acid treatment on thermal degradation kinetics of sugar cane bagasse. Ind Crop Prod. 2015;74:472–7.
40. Gangavati PB, Safi MJ, Singh A, Prasad B, Mishra IM. Pyrolysis and thermal oxidation kinetics of sugar mill press mud. Thermochim Acta. 2005;428:63–70.
41. Coats AW, Redfern JP. Kinetic parameters from thermogravimetric data. Nature. 1964;201:68–9.
42. Agrawal RK, Sivasubramanian MS. Integral approximations for nonisothermal kinetics. AIChE J. 1987;33(7):1212–4.
43. Freeman ES, Carroll B. The application of thermoanalytical techniques to reaction kinetics: the thermogravimetric evaluation of the kinetics of the decomposition of calcium oxalate monohydrate. J Phys Chem. 1958;62(4):394–7.
44. Horowitz HH, Metzger G. A new analysis of thermogravimetric traces. Anal Chem. 1963;35(10):1464–8.
45. Reich L, Stivala SS. Computer-determined kinetic parameters from TG curves. Thermochim Acta. 1980;36:103–5.
46. Piloyan GO, Novikova OS. DTA and TG determination of activation energy for dissociation processes. Zh Neorg Khim. 1967;12:602–4.
47. Jesus HC, Costa EA, Mendonça ASF, Zandonade E. Distribuição de metais pesados em sedimentos do sistema estuarino da ilha de Vitória-ES. Quim Nova. 2004;27(3):376–86.
48. Silva DR, Crespi MS, Crnkovic PCGM, Ribeiro CA. Pyrolysis, combustion and oxy-combustion studies of sugarcane industry wastes and its blends. J Therm Anal Calorim. 2015;121:309–18.
49. Eaton AD, Clesceri LS, Greenberg AE. Standard methods for the examination of water and wastewater. Am Public Health Assoc. 1995;1:106–14.
50. Demirbas A, Gullu D, Çaglar A, Akdeniz F. Estimation of calorific values of fuels from lignocellulosics. Energy Sour. 1997;19:765–70.
51. Cai J, Liu R. Kinetic analysis of solid-state reactions: a general empirical kinetic model. Ind Eng Chem Res. 2009;48:3249–53.
52. Hugot E. Handbook of cane sugar engineering. Amsterdam: Elsevier Science; 1986. p. 1186.